JOURNAL OF MATERIALS SCIENCE **38** (2003) 4573–4579

Synthesis, structure and intercalation of brannerite $LiWVO_6$ wet-chemical products

N. AMDOUNI
Laboratoire des Milieux Désordonnés et Hétérogènes, CNRS-UMR7603, Université Pierre et Marie Curie, 4 place Jussieu, 75252 Paris cedex 05, France; Laboratoire de Chimie des Matériaux, Faculté des Sciences de Tunis, Université de Tunis El Manar, Campus Universitaire, 2092 El Manar II, Tunisia

H. ZARROUK, C. M. JULIEN
Laboratoire des Milieux Désordonnés et Hétérogènes, CNRS-UMR7603, Université Pierre et Marie Curie, 4 place Jussieu, 75252 Paris cedex 05, France
E-mail: cjul@ccr.jussieu.fr

The brannerite-type vanadate $LiWVO_6$ samples were prepared by different synthesis methods including both solid-state reaction of oxides and wet chemistry in aqueous solutions. The physicochemical and electrochemical properties of $LiWVO_6$ products were extensively investigated. Thermal (TG-DTA) analyses and XRD data showed that the powders grown with the quasi-layered structure (C2 space group) have been obtained at temperature below 400°C by the acidification reaction of the aqueous solution. The local structure was characterized by Raman scattering and FTIR spectroscopy. The discharge-charge profiles were evaluated in rechargeable $Li/LiClO_4 + PC/LiWVO_6$ cells and cyclability were estimated in the potential range 3.6–1.4 V. The $LiWVO_6$ positive electrodes fired at 500°C exhibited a fair cycling behavior with a capacity retention of ~164 mAh/g up to the 40th cycle.

1. Introduction

Several vanadate compounds have been of special interest as positive electrode materials for rechargeable lithium batteries [1] because of their open structure and the high valence state of the vanadium ions. These include V_2O_5 [2], V_6O_{13} [3], LiV_3O_8 [4], $LiNaV_2O_5$ [5], etc. Consequently, it is interesting to investigate the electrode behaviour, especially the intercalation and deintercalation of Li ions in the materials containing vanadium ion in different oxidation states. However, the structural arrangement of VO_6 octahedra plays an important role for their ability to intercalate Li ions. For example, rutile-like VO_2 shows poor characteristics for Li insertion, while the more open structure of VO_2(B) with a monoclinic symmetry is able to insert 0.5Li/V at room temperature [6].

$LiWVO_6$ crystallizes with the $ThTi_2O_6$ brannerite-type structure [7]. The brannerite-type $AWVO_6$ compounds (A = Na, K, Li), were first synthesized by Galy *et al*. [8, 9]; they can be depicted as a quasi-layered structure. The AV_2O_6 structure is composed of anionic sheets of VO_6 octahedra sharing three edges. By replacing pentavalent V^{5+} ions with hexavalent W^{6+} ions, monovalent Li^+ ions can be accommodated in the structure. Galy *et al*. have described these vanadate compounds in the monoclinic system, C2 space group ($Z = 2$), with lattice parameters $a = 9.347$ Å, $b = 3.670$ Å, $c = 6.593$ Å, $\beta = 111°83$ for $LiWVO_6$ [8–10]. In this structure the VO_6 octahedra, sharing opposite corners, form chains parallel to the *a* axis. The lengths of the V–O bonds form nearly –V–O–V–O–V– rows along these chains. VO_6 octahedra of the adjacent chains share edges, this forming anionic sheets parallel to the (001) plane. The Li atoms are situated between anionic sheets in LiO_6 octahedra forming chains paralleling the *b* axis, and not linked to one another (Fig. 1). As a result of this structural description, it could be interesting to study the electrode behavior of $LiWVO_6$, especially the intercalation-deintercalation reaction of Li ions.

Recently, Gopalakrishnan *et al*. [11] have grown brannerites $LiMVO_6$ (M = W, Mo) by solid-state reaction and studied their electronic properties. Sakaebe *et al*. have investigated the rate properties of $LiMoVO_6$ as positive electrode for solid-polymer batteries at elevated temperatures [12]. They indicated that discharge capacity strongly depends on temperature and reported an excess of 250 mAh/g between 1.5 and 3.8 V in conventional lithium cell.

In this work, we have attempted to synthesized brannerite-type vanadates $LiWVO_6$ by various high- and low-temperature routes. Their structural characterization has been carried out by X-ray powder diffractometry (XRPD), Raman scattering (RS) and Fourier transform infrared (FTIR) spectroscopies. The electrochemical features of $LiWVO_6$ grown by wet

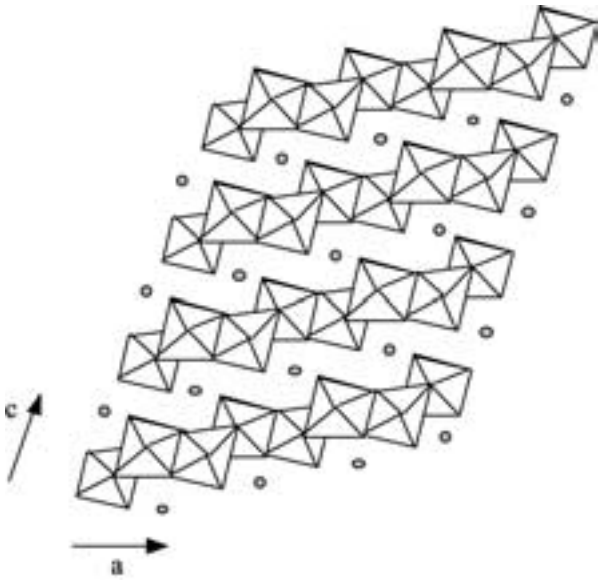

Figure 1 Polyhedral view of the brannerite structure of $LiWVO_6$. Filled circles in the interlayer space represent the Li atoms.

chemistry have been tested in lithium rechargeable batteries.

2. Experimental

2.1. Synthesis

$LiWVO_6$ samples were synthesized by two different techniques. Sample (A) was grown by a solid-state reaction technique at high temperature consisting in the synthesis of $LiWVO_6$ compounds from the mixture of primary oxides V_2O_5, WO_3 and Li_2CO_3. Sample (B) was synthesized using the wet-chemistry technique reported by Julien *et al*. [13]. This low-temperature method consists in the acidification of starting salt materials such as lithium nitrate ($LiNO_3$), ammonium metavanadate (NH_4VO_3) mixed with tungstic acid. The aqueous solution of the above salts was acidified with a solution of an amino-acetic acid, i.e., glycine NH_2CH_2COOH, to induce the decomposition reaction. The precursor thus produced at 400°C was calcined at 550°C to improve the crystal structure.

2.2. Instruments

The thermal decomposition behaviour of the precursor was examined by means of thermogravimetry (TG) and differential thermal analysis (DTA) using an analyser (model Setaram 92) with the simultaneous recording of weight losses (gravimetric thermal analysis) and temperature variations (differential scanning calorimetry). X-ray diffraction patterns were obtained with a Philips X-ray diffractometer (model PW1710) using nickel-filtered Cu K_α radiation ($\lambda = 1.5406$ Å). The diffraction patterns were taken at room temperature in the range of $10^\circ < 2\theta < 80^\circ$ using step scans. The step size and the scan rate were set at 0.1 and 0.2 degree/min, respectively. The particle morphology of the $LiWVO_6$ powders was examined by scanning electron microscopy (SEM, Philips XL30).

Infrared absorption spectra were recorded at room temperature using a Fourier transform interferometer (model Bruker IFS113v). This vacuum bench apparatus was equipped with a Mylar 3.5 μm-thick beamsplitter, a globar source, and a DTGS/PE far-infrared detector. Samples were ground to fine powders dispersed into ICs pellets which are transparent media in the investigated wavenumber range. Data were collected in transmission mode at a spectral resolution of 2 cm^{-1} after 256 scans in vacuum atmosphere. RS spectra of the samples were collected with a double monochromator (Jobin-Yvon model U1000) using the 514.5 mn laser line from the Spectra-Physics 2020 Ar-ion laser. A backscattering geometry was employed and care was taken to use a low excitation power, i.e., below 25 mW, to prevent photodecomposition or reduction of materials by the laser beam during collection of Raman spectra.

Electrochemical studies were carried out on the synthesized products annealed at 550°C to test their suitability as cathode-active materials in lithium-containing batteries. The laboratory-scale Li//$LiWVO_6$ cells were fabricated employing a non-aqueous electrolyte prepared by dissolving 1*M* $LiClO_4$ in propylene carbonate (PC). The typical composite cathodes consisted of the mixture of active $LiWVO_6$ powders, acetylene black, and colloidal PTFE binder in the 90:5:5 weight ratio. The PTFE-acetylene black was used to provide good electrical conductivity as well as mechanical toughness between active grains. The above mixture was pressed on to an expanded aluminium microgrid at a pressure of 500 MPa. This procedure yielded circular pellet electrodes of 10 mm diameter. The pellets were then dried at 120°C in air. Celgar membrane was used as the separator between the cathode and the anode. Electrodes and separators were soaked in the electrolyte before being housed in a Teflon laboratory-cell hardware. In order to assess their electrochemical performance, galvanostatic charge-discharge cycles were recorded using a Mac-Pile apparatus at a slow scan mode (i.e. current pulse of 0.05 mA/cm^2 for 1 h followed by relaxation period of 0.5 h) in the potential range between 1.4 and 3.6 V.

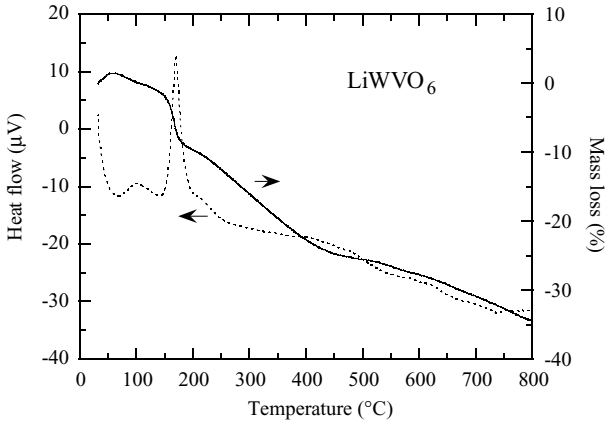

Figure 2 TG-DTA curves of the $LiWVO_6$ powder grown by the glycine acid-assisted combustion technique. These measurements were carried out at a heating rate of 10°C/min with oxygen flow. Full line corresponds to the gravimetric thermal curve and dashed line represents the differential scanning calorimetry curve.

3. Results and discussion

3.1. Synthesis and thermal analysis

Fig. 2 shows the TG-DTA curves which display the formation temperature of the $LiWVO_6$ powders grown by the wet-chemical technique using tungstic acid as W raw material. These measurements were carried out at a heating rate of 10°C/min with oxygen flow. The full line corresponds to the gravimetric thermal curve and the dashed line represents the differential scanning calorimetry curve. A strong exothermic peak appears around 180°C after the departure of the remaining water molecule at ca. 150°C. The formation temperature of the oxide precursor prepared from the wet-chemical method occurs at the low temperature of 400°C for $LiWVO_6$. The exothermic feature corresponds to the combustion of ammonium metavanadate, tungstic acid, and organic species. About 40% of the weight loss occurs during this stage because of a violent oxidation-decomposition reaction. During the combustion process, the yellow-orange solution turned into violet-coloured gel then burnt to give yellowish powder. Assuming that glycine provides combustion heat for calcination in the synthesis of oxide powders, it appeared that this carboxylic acid acts as a fuel during the pyrolysis of the precursor, accelerating the decomposition of ammonium ions in the process. Even though the crystallisation starts around 400°C; thus well-crystallised phases have been obtained for precursor fired at 550°C for 6 h. While the pyrolysis at this stage was very complicated, it could be presumed that the last weak exothermic feature at ca. 440°C in the DTA curve corresponds to the crystallisation of the $LiWVO_6$ brannerite phase.

3.2. Structure and morphology

X-ray diffraction analysis was carried out on the sol-gel synthesized powders at various preparation stages of $LiWVO_6$ to monitor the phase stability of these products. Fig. 3 shows the X-ray diffraction patterns of $LiWVO_6$ powders prepared by the two techniques of synthesis (samples A-B). XRD peaks were indexed assuming the C2 symmetry that corresponds to the monoclinic sitting of the brannerite structure. Lattice parameters of the $LiWVO_6$ calculated by least-squares refinement are listed in Table I. For the sample (B) synthesized by wet-chemical method, we obtained $a = 9.343 \pm 0.002$ Å, $b = 3.672 \pm 0.001$ Å, $c = 6.589 \pm 0.003$ Å and $\beta = 111°60$. The intensity ratio $I(201)/I(001)$ of 1/2 indicates a well-developed brannerite structure. These results are in good agreement with values reported in the literature [8]. It is assumed that the $LiWVO_6$ structure is built by layers parallel to the xOy plane; lithium ions are in octahedral sites between $(WO_6,VO_6)_n$ infinite slabs formed by edge-sharing VO_6 and WO_6 octahedra. Lithium ions occupy the 2*a* sites, while W and V cations are located in 4*i* sites of the brannerite framework.

TABLE I Lattice parameters of $LiWVO_6$ samples (monoclinic C2 S.G.)

Technique	Sample	*a* (Å)	*b* (Å)	*c* (Å)	β
Solid state	A	9.346	3.669	6.591	111°56
Wet chemistry	B	9.343	3.672	6.589	111°60

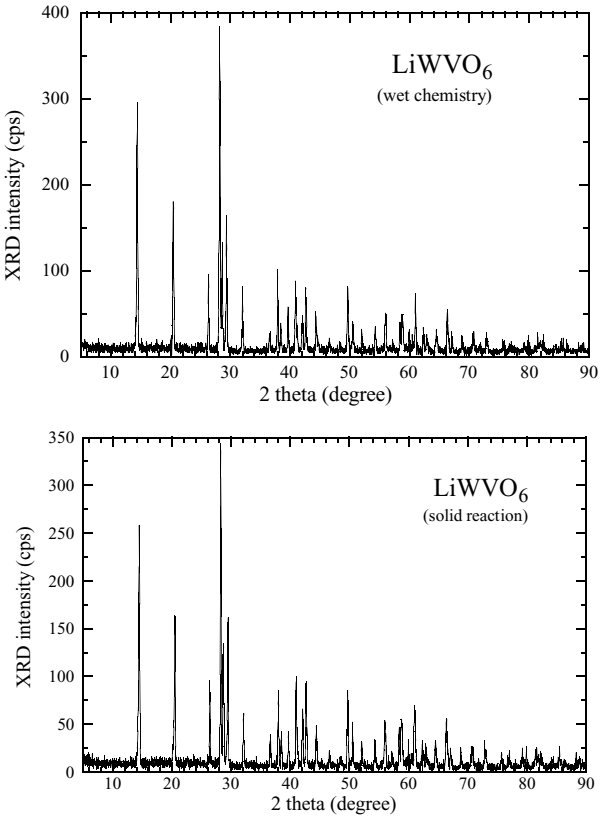

Figure 3 X-ray diffraction patterns of $LiWVO_6$ powders prepared by solid state reaction (A) and wet chemistry (B). XRD peaks were indexed assuming the C2 symmetry (monoclinic sitting of the brannerite structure).

According to the general features of brannerite-type MV_2O_6 metavanadates, it is evident that the conformation of the $LiWVO_6$ system can be described by means of the following building units: (a) the infinite —V—O—W—O—V— chains which run along the $(W,V)O_6$ octahedra, (b) the terminal V=O groups which ensure the weak bonding forces between sheets and thus the layered structure, (c) the double $(V,W)_2O_2$ bridges generated by the edge-sharing between pairs of octahedra, (d) oxygen atoms shared by three different transition-metal atoms, and (e) LiO_6 octahedra.

Fig. 4 shows typical SEM micrographs of $LiWVO_6$ samples prepared by combustion method using tungstic acid. This set presents images with two different magnifications. Because it is known that decreasing particle size leads to increasing reactivity of oxide powders towards oxygen [14], we attribute the well-defined brannerite structure to the optimal synthetic conditions with the use of glycine as chelating agent.

The effect of the synthesis at moderate temperature on the microstructure is clearly depicted when we compare the morphology of powders prepared by the the wet-chemical method assisted by glycine as chelating agent with those prepared by the solid-state reaction (not shown here). The SEM micrographs of the former oxides show that the particles have regular shape with roundness of the edges. The grains are micronmeter sized in diameter with a homogeneous size distribution. The wet-chemical synthesis used leads to powder

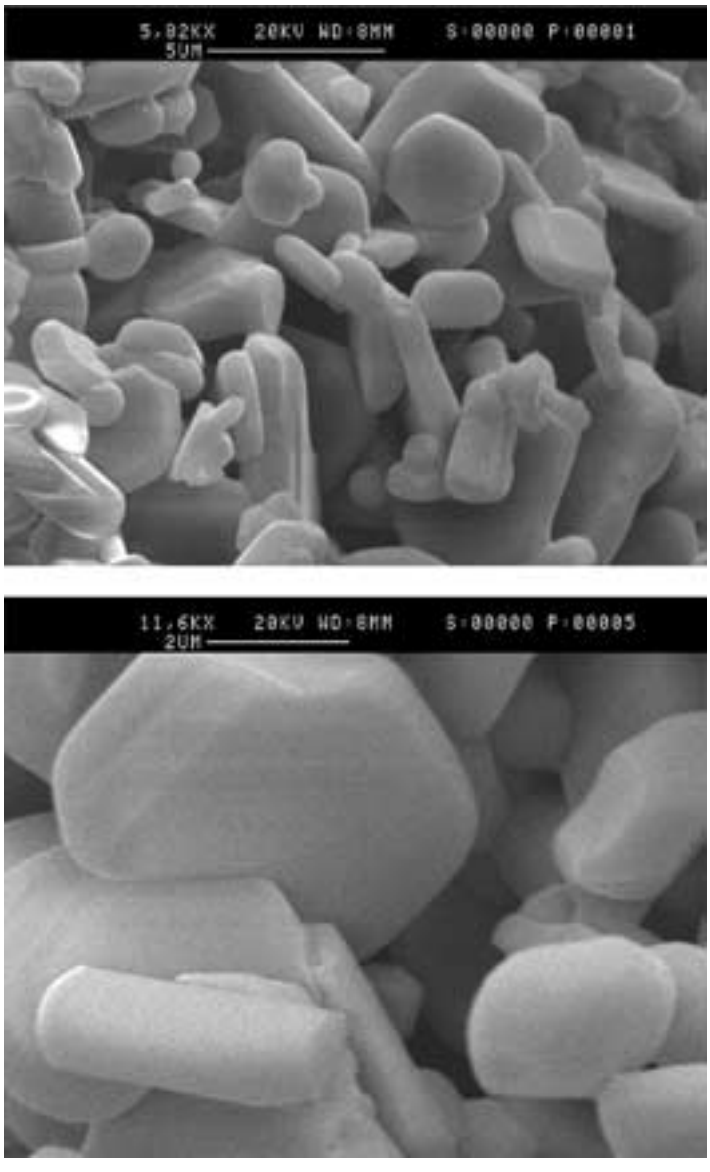

Figure 4 Typical SEM micrographs of $LiWVO_6$ samples prepared by wet-chemical synthesis using tungstic acid.

samples having particle size smaller than that of powders prepared at high temperature from solid-state reaction. Such a behavior is a general trend for samples grown by low-temperature technique. It has been observed for numerous oxides such as lithium cobaltates and lithium manganates [15–17].

The marked decrease in the particle size of $LiWVO_6$ oxides is then unequivocally correlated with kinetics of grain formation using a wet-chemical synthesis assisted by carboxylic acid. Different possibilities can be considered: (i) conditions under which hydrolysis and condensation of the precursor species take place in a weak acidic medium (pH $\approx$ 4.5), (ii) fast kinetics of grain formation with the use of glycine, and (iii) strong exothermic reaction during the salt decomposition around 180°C. The homogeneous cations mixing of Li and (W,V) in the initial emulsion favours the tendency of small grains. Since electrochemical lithium intercalation and deintercalation are in general limited by the rate of diffusion, the aforementioned features are important since smaller grain size can favor the lithium-ion mobility in the particles by reducing the ion-diffusion pathway.

3.3. Vibrational properties

Raman and infrared spectroscopy are sensitive to the short-range environment of oxygen coordination around the cations in both tetrahedral and octahedral crystal sites. Contrary to the diffraction data, which give an average of similar interplanar spacing, the vibration spectrum is a superposition of the spectra of all local structures. The bands in IR and Raman are sensitive to coordination geometry and oxidation states, and remain relatively unaffected by the degree of long-range order.

Figs 5 and 6 show the typical FTIR and Raman spectra, respectively, of $LiWVO_6$ samples calcined at 550°C grown by both solid-state reaction and wet chemistry. The vibrational spectra of the two investigated vanadates are very similar in band position, intensity and shape owing to a well-developed local structure. Table II presents the measured line positions and the assignments proposed on the basis of the constituent building units mentioned above.

Infrared and Raman features show the vibrational modes of the various XO_6 octahedral units building the lattice. Considering that the $LiWVO_6$ phase crystallizes

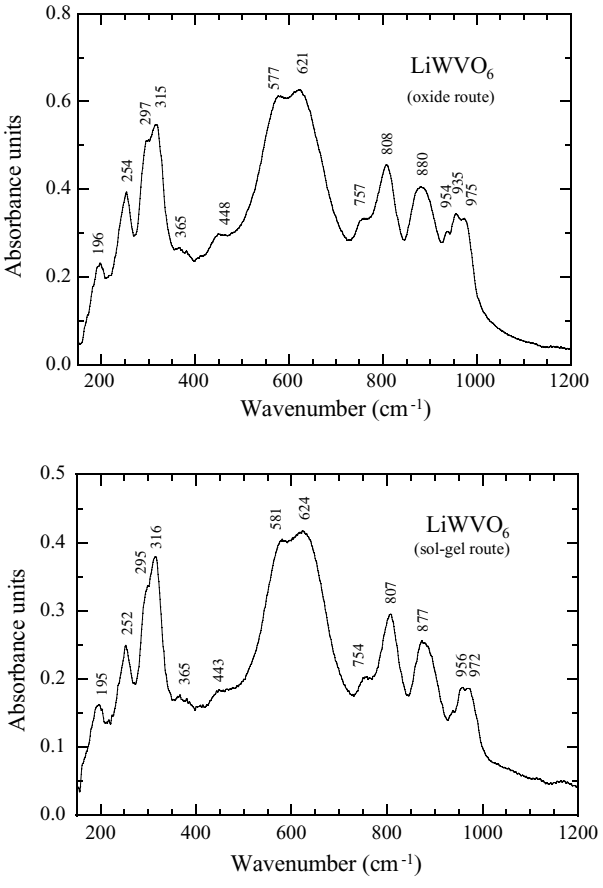

Figure 5 FTIR absorption spectra of $LiWVO_6$ samples as a function of the synthesis method.

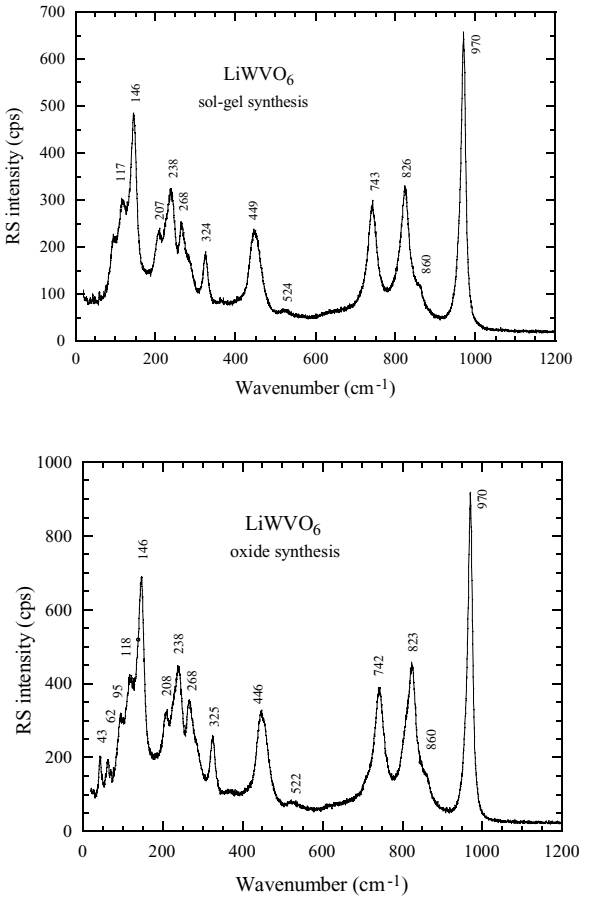

Figure 6 Raman scattering spectra of $LiWVO_6$ samples as a function of the synthesis method.

TABLE II Observed Raman and infrared frequencies and band assignments for the intestigated $LiWVO_6$ vanadates

Frequency (cm^{-1})			
Raman	IR	Intensity	Assignment
117		s	lattice modes
146		vs	
	195	w	
208		m	
238		m	
268	252	m, m	δ(MOM) + $\nu(LiO_6)$
	295	s	
325	316	m, s	δ(MOM)
	365	w	
446	443	w	ν_s(MOM)
522		w	
	581	vs	$\nu(V_2O_2)$
	624	vs	
742	754	s	
823	807	s,s	ν_{as}(VOV)
860	877	s	
	956	w, w	ν(W═O)
970	972	vs, w	ν(V═O)

in the monoclinic system, C2 space group, the group-factor analysis of the spectroscopic symmetry C_2^3 allows the classification for Raman-active ($7A_g + 6B_g$) and infrared-active modes ($4A_u + 11B_u$) [18]. The stretching modes of $(W,V)O_6$ octahedra appear in the high-frequency region (700–1000 cm^{-1}). The most intense Raman line corresponds, undoubtedly, to the terminal V═O species. These possess very strong vanadium-oxygen bonds with V─O distances ranging between 1.61 and 1.69 Å in the brannerite vanadates [18]. The frequency of this line is slightly lower than that observed for the terminal groups in the V_2O_5 oxide [19] in which the V─O distances are shorter. The broadness of the high-frequency band is explained in terms of asymmetrical bonding in the distorted VO_6 octahedra associated with the presence of the terminal W═O groups which appears at 970 cm^{-1}. Two Raman peaks are assigned to the stretching vibrations of the V─O─V bonds, running parallel to the b axis. One of them is located at 823 cm^{-1} and the other at 446 cm^{-1} corresponding to the antisymmetric and symmetric vibration, respectively. A detailed interpretation of the medium-frequency region (300–400 cm^{-1}) of the IR spectrum is difficult because different types of vibrations exist in this spectral domain, involving simultaneously significant displacements of octahedral cations. However, the infrared bending modes of W─O─W and V─O─V bonds are located in the medium-frequency region with a dominant band located at 568 cm^{-1} originates mainly from the W─O─W vibrations. As the metal-oxygen distance ranges from 1.63 to 2.4 Å, this broad band includes many components. In the infrared low-frequency region, we observed a band centered at 250–320 cm^{-1} with three components at 252, 295 and 316 cm^{-1} which are expected to be Li─O stretching and M─O─M bending motions. It is difficult to ensure the purity of each modes because, owing the condensed nature of the structure, considerable mixing between some of them cannot be excluded. Such mixings are undoubtedly important in the spectral region

below 400 cm^{-1}. Nevertheless, one of the main contribution is attributed to the stretching mode of LiO_6 units. It is a general rule for inorganic oxides that the band related to the vibration of an isolated LiO_6 octahedron appears in the far-infrared domain between 200–300 cm^{-1} [20]. Thus, the band at 252 cm^{-1} is assigned with confidence to an asymmetric stretching vibration of LiO_6. The lines below 200 cm^{-1} are attributed to the external (lattice) modes. The two intense Raman lines at 118 and 146 cm^{-1} correspond to the vibration of $\delta(M_2O_2)_n$ chains. These modes are observed at 104 and 145 cm^{-1} in V_2O_5 oxide. In conclusion, the local structure of samples grown by glycine-assisted wet-chemistry technique is in good accordance with the model of octahedral occupancy for lithium cations in the interlayer space. This is of great importance for the intercalation-deintercalation reactions since lithium cations could have high mobility in such a structure.

3.4. Electrochemical properties

Fig. 7 illustrates the first discharge-charge cell voltage for the $LiWVO_6$ brannerite. The lithium intercalation reaction in Li_xWVO_6 occurs at potentials below 3.0 V. The quasi-OCV curves were recorded after each relaxation period presented in the potential range 3.6–1.4 V for Li//$LiWVO_6$ cells using positive electrode grown by the combustion method. A fresh assembled electrochemical cell delivers a potential of 3.65 V vs. Li/Li^+. As lithium ions are inserted in the $LiWVO_6$ matrix, the discharge process exhibits a voltage profile typical for lithiated oxides. Two steps are observed in the compositional range $0.0 \leq x \leq 2.5$. The cell potential value of 1.65 V is attained when 2.4 Li/V are intercalated in the octahedral sites of the $LiWVO_6$ framework. The discharge curve of the Li//$LiWVO_6$ freshly assembled cell initially showed a quasi-plateau developed around 2.3 V followed by a gradual falling slope up to $x = 1.0$. We believe this plateau indicates the existence of a two-phase region and the gradual slope, a homogeneous single-phase region, that is the formation of a lithium intercalation compound. Considering a voltage limit of 1.5 V at the end of the first discharge,

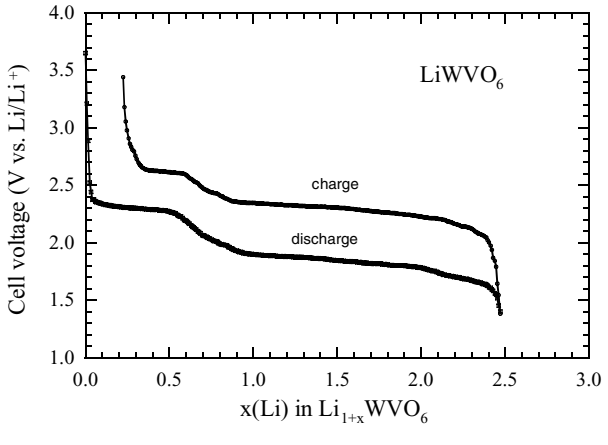

Figure 7 First discharge-charge profiles of a Li//$LiWVO_6$ cell obtained at current density 0.05 mA/cm^2. Positive electrode material was prepared by the combustion method (sample B).

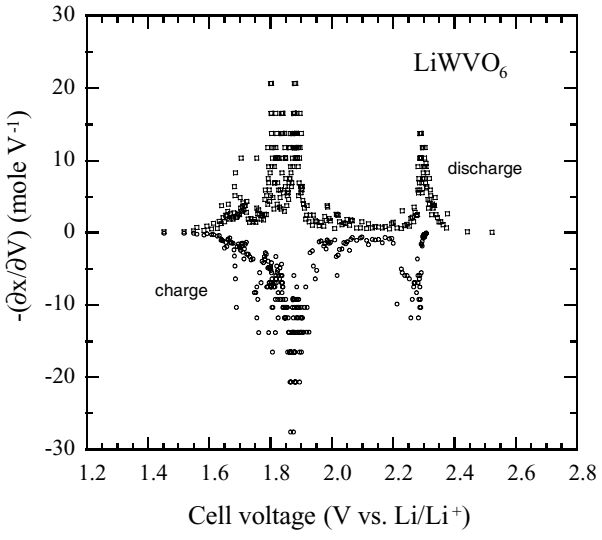

Figure 8 Incremental capacity $-\partial x/\partial V$ of $Li_{1+x}WVO_6$ intercalated by lithium in the range $0.0 \leq x \leq 2.5$.

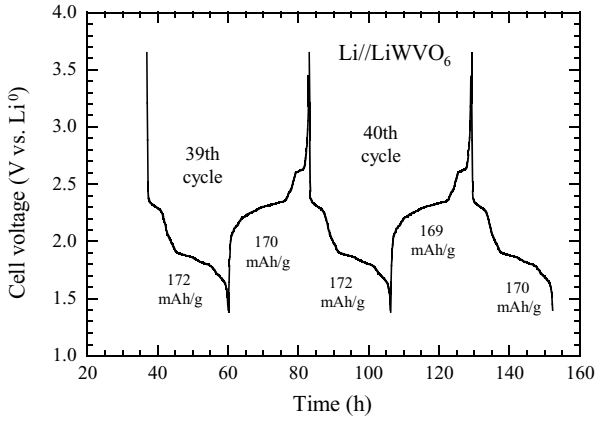

Figure 9 Cyclic behavior the Li//$LiWVO_6$ cell using the positive electrode material prepared by the sol-gel method (sample B). Charge and discharge were obtained at current density 0.05 mA/cm^2.

the gravimetric capacity stored in the Li//$LiWVO_6$ cell is about 195 mAh/g. This is in agreement with recent preliminary data [21].

Fig. 8 shows the incremental capacity $(-\partial x/\partial V)$ of Li_{1+x} WVO_6 intercalated by lithium in the range $0.0 \leq x \leq 2.5$. Plateaus in voltage versus capacity give rise to peaks in $-(\partial x/\partial V)$; so derivative plots are useful for displaying details. From the results shown in Fig. 7, for the region I corresponding to the upper voltage plateau, a two-phase system is recognised, whereas the region II can be attributed to a single phase characterized by an S-shaped curve in the voltage profile. The two regimes of intercalation are clearly depicted when incremental capacity $-(\partial x/\partial V)$ is plotted vs. cell voltage (Fig. 8). The band centered at 1.85 V (capacity around $x = 1.5$) is indicative of the one-phase system, while the sharp band at 2.30 V (capacity around 0.4) is indicative of the two-phase system.

Fig. 9 displays the cyclic behavior of the Li//$LiWVO_6$ cell using a positive electrode material prepared via sol-gel method (sample B). Charge and discharge were obtained at current density 0.05 mA/cm^2. Considering that the theoretical capacity is 79.3 mAh/g for

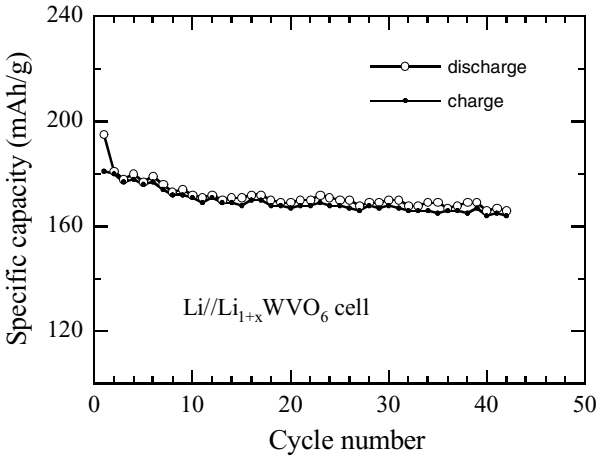

Figure 10 Capacity vs. cycle number for $Li//Li_{1+x}WVO_6$ cell.

$\Delta x = 1$, insertion of 2.5 Li/V yields a capacity of 195 mAh/g which 98% of the theoretical value. Fig. 10 shows variation of the capacity vs. cycle number for $Li//Li_{1+x}WVO_6$ cell. The shape of the charge-discharge curves shows a fair reversibility and capacity retention at the 40th cycle. These studies demonstrate that cathodes yield capacities around 164 mAh/g for $LiWVO_6$ when discharged to a cut-off voltage of 1.5 V. There is an $\sim$10% loss of capacity for the first charge and discharge cycle. The sharp drop in discharge capacity that occurs between cycle 1 and 2 (Fig. 10) appears to be related to the conditioning and stabilization of $LiWVO_6$ electrode and is speculated to result from the deactivation of the electrode surface. Thereafter, the capacity decreases slightly from 180 mAh/g (2nd cycle) to 164 mAh/g (43rd cycle).

4. Conclusion

This work has shown that low temperature using an aqueous combustion process is able to grown $LiWVO_6$ single phase. The wet-chemical method, in which glycine acts such as a fuel, provides micron-sized particles which are adequate for fast lithium intercalation-deintercalation reactions occurring in rechargeable lithium cells. The use of solution processing leads to molecular level mixing and highly uniform materials. The low-temperature technique adopted for the synthesis $LiWVO_6$ cathode materials has yielded particles with grain size in the range 1–2 μm, which favour good electrochemical performance. The first charge-discharge voltage profiles demonstrated that the positive electrodes yield capacity of 195 mAh/g when discharged to a cut-off voltage of 1.5 V ($0.0 \geq x \geq 2.5$) in $Li//Li_{1+x}WVO_6$ cells. Subsequent cycling measurements show a capacity retention of 164 mAh/g up to the 40th cycle.

References

1. C. JULIEN and G. A. NAZRI, "Solid State Batteries, Materials Design and Optimization" (Klumer, Boston, 1994).
2. D. W. MURPHY, P. A. CHRISTIAN, F. J. DISALVO and J. V. WASZCZAK, *Inorg. Chem.* **18** (1979) 2800.
3. D. W. MURPHY, P. A. CHRISTIAN, F. J. DISALVO, J. N. CARIDES and J. V. WASZCZAK, *J. Electrochem. Soc.* **128** (1981) 2053.
4. G. PISTOIA, M. PASQUALI, G. WANG and L. LI, *ibid.* **137** (1990) 2365.
5. L. BOUHEDJA, S. CASTRO-GARCIA, J. LIVAGE and C. JULIEN, *Ionics* **4** (1998) 227.
6. B. ZACHAU-CHRISTIANSEN, K. WEST and T. JACOBSEN, *Mater. Res. Bull.* **20** (1985) 485.
7. R. RUH and A. D. WADSLEY, *Acta Crystallogr.* **21** (1966) 974.
8. J. GALY, J. DARRIET and B. DARRIET, *C. R. Acad. Sci. (Paris)* **C264** (1967) 1477.
9. J. GALY, G. MEUNIER, J. SENEGAS and P. HAGENMULLER, *J. Inorg. Nucl. Chem.* **33** (1971) 2403.
10. B. DARRIET and J. GALY, *Bull. Soc. Fr. Mineral. Crystallogr.* **91** (1968) 325.
11. J. GOPALAKRISHNAN, N. S. P. BHUVANESH, R. VIJAYARAGHAVAN and N.Y. VASANTHACHARYA, *J. Mater. Chem.* **7** (1997) 307.
12. H. SAKAEBE, M. SHIKANO, Y. XIA, T. SAKAI, T. ERIKSSON, T. GUSTAFSSON and J. THOMAS, "Extended Abstracts of the 10th Intl. Meeting on Lithium Batteries" (Como, Italy, 2000) Abtr. No. 225.
13. C. JULIEN, C. LETRANCHANT, S. RANGAN, M. LEMAL, S. ZIOLKIEWICZ, S. CASTRO-GARCIA, L. EL-FARH and M. BENKADDOUR, *Mater. Sci. Eng.* B **76** (2000) 145.
14. P. TAILHADES, B. GILOT and A. ROUSSET, *J. Phys.* IV **C1** (1997) 249.
15. C. JULIEN, M. S. MICHAEL and S. ZIOLKIEWICZ, *Intl. J. Inorg. Mater.* **1** (1999) 29.
16. C. JULIEN, L. EL-FARH, S. RANGAN and M. MASSOT, *J. Sol-Gel Sci. & Technol.* **15** (1999) 63.
17. C. JULIEN, S. ZIOLKIEWICZ, M. LEMAL and M. MASSOT, *J. Mater. Chem.* **11** (2001) 1837.
18. E. J. BARAN, C. I. CABELLO and A. G. NORD, *J. Raman Spectrosc.* **18** (1987) 405.
19. I. R. BEATTIE and T. R. GILSON, *J. Chem. Soc.* A (1969) 2322.
20. C. JULIEN, *Solid State Ionics* **136/137** (2000) 887.
21. S. R. S. PRABAHARAN, T. T. YONG, A. FAUZI and M. S. MICHAEL, *J. Power Sources* **97/98** (2001) 535.

Received 29 July 2002
and accepted 7 July 2003